Advances in Applied Mathematics and Mechanics
Adv. Appl. Math. Mech., Vol. **9**, No. 5, pp. 1225-1249

DOI: 10.4208/aamm.2015.m1085
October 2017

A Meshfree Technique for Numerical Simulation of Reaction-Diffusion Systems in Developmental Biology

Zahra Jannesari[1] and Mehdi Tatari[1,2,*]

[1] *Department of Mathematical Sciences, Isfahan University of Technology, Isfahan, 84156-83111, Iran*
[2] *Institute for Research in Fundamental Sciences (IPM), P.O. Box: 19395-5746, Tehran, Iran*

Received 2 May 2015; Accepted (in revised version) 10 November 2016

Abstract. In this work, element free Galerkin (EFG) method is posed for solving nonlinear, reaction-diffusion systems which are often employed in mathematical modeling in developmental biology. A predicator-corrector scheme is applied, to avoid directly solving of coupled nonlinear systems. The EFG method employs the moving least squares (MLS) approximation to construct shape functions. This method uses only a set of nodal points and a geometrical description of the body to discretize the governing equation. No mesh in the classical sense is needed. However a background mesh is used for integration purpose. Numerical solutions for two cases of interest, the Schnakenberg model and the Gierer-Meinhardt model, in various regions is presented to demonstrate the effects of various domain geometries on the resulting biological patterns.

AMS subject classifications: 65M99, 92B99

Key words: Element free Galerkin (EFG) method, reaction-diffusion systems, meshfree methods, MLS approximation, developmental biology.

1 Introduction

1.1 Reaction-diffusion equations

One of the important class of partial differential equations, are reaction-diffusion equations. These equations are frequently encountered in mathematical biology, ecology, chemistry and physics. This type of equations leads to interesting phenomena, such as pattern formation far from equilibrium, shading and pulse splitting. Biologists and

*Corresponding author.
Email: z.jannesari@math.iut.ac.ir (Z. Jannesari), mtatari@cc.iut.ac.ir (M. Tatari)

 ©2017 Global Science Press

https://doi.org/10.4208/aamm.2015.m1085 Published online by Cambridge University Press

mathematicians have explored stable patterns, like spots and stripes by several reaction-diffusion systems. Alan Turing in [41], created a mathematical model describing the growing embryo's sequential changes that occur from fertilization to birth. He defined the mechanism in the context of biological morphogenesis, which showing that reactions between two diffusible chemicals (morphogens) could give rise to spatially heterogeneous concentrations through an instability driven by diffusion. Turing [41], Madzvamuse [24–27] have proposed numerical simulations considering growing dominion conditions and particular geometries modifying distribution patterns. The simplest and most typical Turing reaction-diffusion system consists of two chemical species, usually referred to as activator and inhibitor u and v as follows:

$$\frac{\partial u}{\partial t} = \gamma f(u,v) + \nabla^2 u, \tag{1.1a}$$

$$\frac{\partial v}{\partial t} = \gamma g(u,v) + d\nabla^2 v, \tag{1.1b}$$

where $d = d_v/d_u$ is the relationship between these species diffusion coefficients, while γ is a non-dimension coefficient associated with reactive processes f and g [15] that is proportional to the length of the domain.

In 1952, Turing in [41] suggested that chemicals can react and diffuse to produce patterns. Therefore, the formation of patterns in an organism can be modeled by a series of reaction-diffusion equations for the interacting species. Some authors have been studying another biological situations like animal skin pattern formation [13, 26, 28, 31], bone, tissue and tumor formation [7, 12, 14], animal population distribution [5, 42]. Therefore, different numerical techniques for solution of the reaction-diffusion problem have been implemented, like finite difference methods [4, 8, 20, 31], finite element methods [7, 24, 25], spectral element methods [19], finite volume spectral element method [37] and meshfree finite point method [39]. Many initial studies on Turing pattern formation have been devoted to work on fixed meshes.

The growing nature of reaction-diffusion problems (in a biological context) have led to studies on growing meshes. For example, Madzvamuse [26] has studied the incidence of mesh growth in diffusion formation of pattern. In this seminal work, Madzvamuse suggested an algorithm for 2D diffusion-reaction problem solution using a continuously growing Eulerian dominion. For example, [25] introduced a mesh growing finite element technique application for biological problems.

In this study, a meshfree method for solving the reaction-diffusion system in complex domains is considered.

1.2 A brief review on meshfree methods

Conventional numerical methods such as finite element method (FEM) and finite volume method (FVM) need an a priori definition of the connectivity of the nodes, i.e., these methods rely on a mesh. Mesh generation has always posed challenges for computational scientists, because of its complication and time consuming.

https://doi.org/10.4208/aamm.2015.m1085 Published online by Cambridge University Press

In contrast, a new class of numerical methods has been developed. These methods approximate partial differential equations only by using a set of nodes. Some of these methods are not really meshfree methods, since they use a background mesh for the numerical integration of the weak form. To be a truly meshfree method, both interpolation and integration should be performed without a mesh. The main attractions of meshfree methods are their simplified adaptability, ability to cope with moving boundaries since no remeshing during the calculations is necessary.

There are a number of meshless (or meshfree) methods such as smoothed particle hydrodynamics (SPH) [30, 36], diffuse element method (DEM) [33], reproducing kernel particle method (RKPM) [22, 23], *hp*-clouds method [11], finite point method (FPM) [34, 35], partition of unity method (PUM) [29], local boundary integral equation (LBIE) method [44,45], meshless local Petrov-Galerkin (MLPG) method [2,3]. Finite point method, meshless local Petrov-Galerkin method and local boundary integral equation method are truly meshfree methods. Element free Galerkin (EFG) method which is proposed by Belytschko [6, 10], is not a truly meshfree procedure. The major features of the EFG method are as follows:

- The MLS approximation is used to create the shape functions.
- Galerkin weak form is employed to discretize the governing partial differential equations.
- Cell structure or background mesh for integration are required to carry out integration to calculate matrices system.

In this work the element free Galerkin method is outlined for nonlinear reaction-diffusion systems. The rest of the paper is organized as follows: In the following section some interacting chemical models are briefly described. Section 3 is devoted to time descritization and the element free Galerkin method along with the MLS approximation is described for the proposed problems. Also the predicator-corrector scheme to solve the obtained nonlinear system is outlined in this section. In Section 4 numerical results for some problems involving the Gierer-Meinhardt and Schnakenberg models are presented to confirm the validity of the approach. The last section is a conclusion.

2 Some interacting chemical models

The reaction of the system is based on a basic diffusion equation of the chemical concentration along with an additional nonlinear reaction term. Creating an equation using the vector chemical concentration, $\mathbf{u}$, reaction kinetics $\mathbf{R}(\mathbf{u})$ and diffusivities in a diagonal matrix $\mathbf{D}$ describe the reaction-diffusion system as follows:

$$\frac{\partial \mathbf{u}}{\partial t} = \gamma \mathbf{R}(\mathbf{u}) + \mathbf{D}\nabla^2 \mathbf{u} \quad \text{in } \Omega \times [0,\infty), \tag{2.1}$$

https://doi.org/10.4208/aamm.2015.m1085 Published online by Cambridge University Press

with $\gamma \neq 0$ and some appropriate boundary conditions and initial conditions. If two chemical species

$$\mathbf{u} = \begin{pmatrix} u \\ v \end{pmatrix}$$

are undergoing morphogenesis, it can be generalized that they will have specific positive diffusion coefficients d_1 and d_2 respectively. To specify the two-component model system, the reaction kinetics is defined as follows:

$$\mathbf{R}(\mathbf{u}) = \begin{pmatrix} f(u,v) \\ g(u,v) \end{pmatrix}.$$

Hence the Eq. (2.1) can be written as:

$$\begin{pmatrix} u_t \\ v_t \end{pmatrix} = \gamma \begin{pmatrix} f(u,v) \\ g(u,v) \end{pmatrix} + \nabla^2 \begin{pmatrix} d_1 u \\ d_2 v \end{pmatrix}. \tag{2.2}$$

In Eq. (2.2), the two chemical concentrations, u and v which are dependent on $(\mathbf{x},t)$ have different diffusion coefficients. Depending on the reaction and diffusion of the system, the reaction kinetics can vary. To be well-posedness each PDE requires two boundary conditions. Initial conditions of the solution for the fixed boundary problem are given by $\mathbf{u}(\mathbf{x},0) = \mathbf{u}_0(\mathbf{x})$. These conditions are defined as small random perturbations around the uniform homogeneous steady state, if it exists (i.e., a state $u =$ constant, $v =$ constant satisfying the boundary conditions and Eqs. (2.1)) [26]. The boundary conditions can be of Dirichlet type or of (homogeneous) Neumann type where describe zero-flux of u (or v) out of the boundary. Two different types of reaction kinetics which produce reaction diffusion systems are considered such as activator-inhibitor mechanisms.

2.1 Gierer-Meinhardt system

In 1972 Gierer and Meinhardt [16] proposed the following mathematical model

$$\frac{\partial u}{\partial t} = \gamma \left(a - bu + \frac{u^2}{v(1+ku^2)} \right) + \nabla^2 u, \tag{2.3a}$$

$$\frac{\partial v}{\partial t} = \gamma (u^2 - v) + d\nabla^2 v, \tag{2.3b}$$

which is a non-dimensional reaction-diffusion system of activator-inhibitor type. In this model, reaction kinetics are chosen in such a way that one of the chemicals u (the activator) activates the production of the other chemical v (the inhibitor) which inhibits the production of the activator. Here a, b, d and γ are all non-dimensional positive constant and k is a measure of the saturation concentration (see for example [32]). This model is appeared to account for many important types of pattern formation in development. The biological interpretation of the reaction kinetics follows as above and the nonlinear term $\gamma u^2/\left(v(1+ku^2)\right)$ in Eq. (2.3a) implies autocatalysis in u with saturation at high concentration values of u and inhibition of u through the production of v. In Eq. (2.3b), v is activated (produced) by u and degraded linearly.

https://doi.org/10.4208/aamm.2015.m1085 Published online by Cambridge University Press

2.2 Schnakenberg model

One of the most widely studied and simplest reaction diffusion models in biological Turing-type pattern formation is the Schnakenberg model. This model is based on a hypothetical mechanism consisting of a trimolecular autocatalytic reactions involving two chemicals that proposed by Schnakenberg [38] in 1979. This is a cross activator-inhibitor chemical model and the non-dimensionalized form of the system with a positive diffusion coefficient d for the inhibitor chemical is:

$$\frac{\partial u}{\partial t}=\gamma(a-u+u^2v)+\nabla^2u, \tag{2.4a}$$

$$\frac{\partial v}{\partial t}=\gamma(b-u^2v)+d\nabla^2v. \tag{2.4b}$$

Here a, b are positive constants and γ is a scale parameter defined proportional to the dimensional length of the domain. Also, the reaction terms $(a-u+u^2v)$ and $(b-u^2v)$ are such that a non-zero homogeneous steady state (u_s,v_s) exists (see the next subsection). The biological interpretation of the reaction kinetics in Eqs. (2.4a) and (2.4b) is that u and v are produced at a constant rate γa and γb, respectively, while u is degraded linearly at rate γ. The nonlinear term γu^2v implies the nonlinear activation of u and nonlinear consumption for v [26].

2.3 Linear stability analysis

For any steady state to be driven unstable in the presence of diffusion, there are certain conditions which must be satisfied. To find out what these conditions are, this discussion follows of [32] Chapter 14. The values of γ and d are determined by these conditions. To formulate the problem mathematically, it is necessary to specify initial conditions and boundary conditions. These take to be given initial conditions which are small perturbations about the steady state and zero flux boundary conditions. Therefore, the mathematical problem is

$$\begin{aligned}
&\frac{\partial u}{\partial t}=\gamma f(u,v)+\nabla^2u,\\
&\frac{\partial v}{\partial t}=\gamma g(u,v)+d\nabla^2v,\\
&u(\mathbf{x},0),\ \ v(\mathbf{x},0)\ \ \text{are given and}\quad \begin{pmatrix}\dfrac{\partial u}{\partial n_p}\\[2mm] \dfrac{\partial v}{\partial n_p}\end{pmatrix}=\mathbf{0}.
\end{aligned}$$

Here, n_p is the unit outward normal to $\partial\Omega$ and Ω is the problem domain. In the absence of diffusion any homogenous (positive) steady state must be linearly stable. It is only in

https://doi.org/10.4208/aamm.2015.m1085 Published online by Cambridge University Press

the presence of diffusion that we want this steady state to be driven unstable. If there are no diffusion terms, then

$$\frac{\partial u}{\partial t}=\gamma f(u,v),$$
$$\frac{\partial v}{\partial t}=\gamma g(u,v).$$

It can be derived from chapter 14th of [32] that linear stability is guaranteed if

$$f_u+g_v<0,\quad f_ug_v-f_vg_u>0,$$

where f_u, f_v, g_u and g_v indicate the partial derivatives of the reaction functions regarding concentration variables. These inequalities are satisfied at the steady state (u_s,v_s), in the other words when $(u,v)=(u_s,v_s)$.

To find the steady states of the diffusionless system, putting $f(u,v)=g(u,v)=0$. Therefor, the unique steady state is:

$$u=u_s=a+b,\quad v=v_s=\frac{b}{(a+b)^2}.$$

The above linear stability conditions will put restrictions on the parameter ranges of a and b. It is concerned with positive solutions for the steady states, so

$$b>0,\quad a+b>0.$$

Now, we should look at the full reaction diffusion system and linearise about the steady state again. This will give further conditions on the parameters (this part is omitted just for simplicity, the interested reader can refer to [32]). By do this, the additional restrictions are

$$df_u+g_v>0,\quad (df_u+g_v)^2-4d(f_ug_v-f_vg_u)>0.$$

Consider to the first restriction $f_u+g_v<0$ and $df_u+g_v>0$, this means that f_u and g_v must have opposite signs. It also induces that $d\neq 1$, otherwise it would be impossible to satisfy both inequalities.

From the stability analysis [32] in the unit square with zero flux boundary conditions, the value of the parameters d and γ corresponding to the spatial mode $\cos(m\pi x)\cos(n\pi y)$ denoted by (m,n), are shown in Table 1 which has been extracted from [26]. For some fixed parameter values:

- Schnakenberg model: $a=0.1$, $b=0.9$,
- Gierer-Meinhardt model: $a=0.1$, $b=1.0$, $k=0.5$.

https://doi.org/10.4208/aamm.2015.m1085 Published online by Cambridge University Press

Table 1: Values for d and γ under which a particular mode is isolated on a unit square domain for the Gierer-Meinhardt and Schnakenberg models.

Mode	Gierer-Meinhardt		Schnakenberg	
(m,n)	d	γ	d	γ
(1,0)	520.1573	67	10	29
(1,1)	105.1573	168.8	11.5776	70.6
(2,0)	84.1573	238.26	10	114
(2,1)	77.6473	411.42	9.1676	176.72
(2,2)	75.1573	483.43	8.6676	230.82
(3,0)	70.8473	619.45	8.6176	265.22
(3,1)	72.1573	756.23	8.6676	329.20
(3,2)	73.1573	901.38	8.8676	379.21
(3,3)	70.5573	1266.99	8.6076	535.09
(4,0)	71.1573	1033.51	8.6676	435.99
(4,1)	70.3573	1164.86	8.5876	492.28
(4,2)	71.1573	1519.87	8.7176	625.35
(4,3)	71.1573	1580.66	8.6676	666.82
(4,4)	73.1473	2167	8.6076	909.66

3 The numerical implementation

Two standard species reaction-diffusion systems in the following form are considered to demonstrate objects

$$\frac{\partial u}{\partial t} = \gamma f(u,v) + \nabla^2 u, \tag{3.1a}$$

$$\frac{\partial v}{\partial t} = \gamma g(u,v) + d\nabla^2 v, \tag{3.1b}$$

in $\Omega \times [0,\infty)$, $\Omega \subset \mathbb{R}^2$ with the homogenous Neumann boundary conditions

$$\frac{\partial u}{\partial n_p}(\mathbf{x},t) = 0, \quad \frac{\partial v}{\partial n_p}(\mathbf{x},t) = 0, \quad \mathbf{x} \in \partial\Omega,$$

and the initial conditions

$$u(\mathbf{x},0) = u_0(\mathbf{x}), \quad v(\mathbf{x},0) = v_0(\mathbf{x}), \quad \mathbf{x} = (x,y) \in \Omega.$$

3.1 Time discretization

In order to solve the reaction-diffusion system we first discretize the time derivative, for this a Crank-Nicolson scheme is employed. In this technique, the average of times t and $t+\Delta t$ is considered. Hence the Eqs. (3.1a) and (3.1b) can be written as:

$$u^{(k+1)} - \beta\left(\gamma f(u^{(k+1)},v^{(k+1)}) + \nabla^2 u^{(k+1)}\right) = u^{(k)} + \beta\left(\gamma f(u^{(k)},v^{(k)}) + \nabla^2 u^{(k)}\right), \tag{3.2a}$$

$$v^{(k+1)} - \beta\left(\gamma g(u^{(k+1)},v^{(k+1)}) + d\nabla^2 v^{(k+1)}\right) = v^{(k)} + \beta\left(\gamma g(u^{(k)},v^{(k)}) + d\nabla^2 v^{(k)}\right), \tag{3.2b}$$

https://doi.org/10.4208/aamm.2015.m1085 Published online by Cambridge University Press

in which $u^{(k)}(\mathbf{x})=u(\mathbf{x},k\Delta t)$, $v^{(k)}(\mathbf{x})=v(\mathbf{x},k\Delta t)$ and $\beta=\Delta t/2$.

3.2 The EFG method

The element free Galerkin (EFG) method employs moving least squares (MLS) approximation to construct the meshfree shape function and uses the weak form of the problem to discretize the governing partial differential equations.

In this subsection at first a brief summary about the MLS approximation is given, after that the weak form and the governing system is derived.

3.2.1 The MLS approximation

The MLS approximation is usually considered to be one of the best schemes to approximate data with reasonable accuracy. This approximation, introduced by Lancaster and Salkauskas [21] is local. At any arbitrary evaluation point $\mathbf{x}$, only the neighboring nodes in whose domain of influence point $\mathbf{x}$ resides are consequential. The influence of a node $\mathbf{x}_i$ is governed with a decreasing weight function $w(\mathbf{x}-\mathbf{x}_i)$, which vanishes outside the domain of influence of node $\mathbf{x}_i$. consider to find an approximate solution $u_h^{(k)}(\mathbf{x})=u(\mathbf{x},k\Delta t)$ in the problem domain $\bar{\Omega}$, while the true solution $u^{(k)}$ is known at some selected points $\mathbf{x}_i$. Then in a least squares sense, the objective is to find minimization of the expression $(u_h^{(k)}(\mathbf{x}_i)-u^{(k)}(\mathbf{x}_i))^2$ for each i. Let the approximation $u_h^{(k)}(\mathbf{x})$ for the solution $u^{(k)}(\mathbf{x})$, is posed as a polynomial of order m with nonconstant coefficients. For example in 2 dimension, for a linear basis $u_h^{(k)}(\mathbf{x})$ is written as

$$u_h^{(k)}(\mathbf{x})=a_0^{(k)}(\mathbf{x})+xa_1^{(k)}(\mathbf{x})+ya_2^{(k)}(\mathbf{x}),\quad \forall\mathbf{x}\in\bar{\Omega}.$$

The approximation can be written in matrix form

$$u_h^{(k)}(\mathbf{x})=\mathbf{p}^T(\mathbf{x})\mathbf{a}^{(k)}(\mathbf{x}),\quad \forall\mathbf{x}\in\bar{\Omega}, \tag{3.3}$$

where $\mathbf{p}^T(\mathbf{x})=[p_1(\mathbf{x})\ p_2(\mathbf{x})\ \cdots\ p_m(\mathbf{x})]$ is a complete polynomial of order m. In 2 dimensional, linear base and quadratic base are defined as following respectively:

$$\begin{aligned}&\mathbf{p}^T(\mathbf{x})=[1\ x\ y]\ \text{ linear basis,} && m=3,\\ &\mathbf{p}^T(\mathbf{x})=[1\ x\ y\ x^2\ xy\ y^2]\ \text{ quadratic basis,} && m=6.\end{aligned}$$

The vector $a^{(k)}(\mathbf{x})$ is given by

$$\mathbf{a}^{(k)}(\mathbf{x})=[a_0^{(k)}(\mathbf{x})\ a_1^{(k)}(\mathbf{x})\ \cdots\ a_m^{(k)}(\mathbf{x})]^T.$$

The unknown parameters $a_j^{(k)}(\mathbf{x})$, $j=0,1,\cdots,m$, vary with space coordinates $\mathbf{x}$. To determine the unknown parameters $a_j^{(k)}(\mathbf{x})$ at any given point $\mathbf{x}$, the least squares functional

https://doi.org/10.4208/aamm.2015.m1085 Published online by Cambridge University Press

is written with the approximation substituted in, for $u_h^{(k)}(\mathbf{x})$ as following:

$$\mathcal{J}(\mathbf{x})=\frac{1}{2}\sum_{i=1}^{N_t}\left(\mathbf{p}^T(\mathbf{x}_i)\mathbf{a}^{(k)}(\mathbf{x})-u^{(k)}(\mathbf{x}_i)\right)^2, \tag{3.4}$$

where N_t is the total number of points. It should be noted that the coefficient $1/2$ is added for mathematical convenience. The local solution is influenced by the local nodes and nodes far away have not influence. Hence each summation term, in the least squares functional is weighted by a weight function $w(\mathbf{x}-\mathbf{x}_i)$, which limits the term's influence to node $\mathbf{x}_i$ and several surrounding nodes. Based on this intuition the functional $\mathcal{J}$ is modified to a weighted least squares functional as follows:

$$\mathcal{J}(\mathbf{x})=\frac{1}{2}\sum_{i=1}^{N_t}w(\mathbf{x}-\mathbf{x}_i)\left(\mathbf{p}^T(\mathbf{x}_i)\mathbf{a}^{(k)}(\mathbf{x})-u^{(k)}(\mathbf{x}_i)\right)^2. \tag{3.5}$$

Next, it is necessary to minimize $\mathcal{J}$ with respect to each $a^{(k)}(\mathbf{x}_i)$. It is helpful to first write the functional in matrix form. Therefore, the functional $\mathcal{J}$ is written as follows:

$$\mathcal{J}(\mathbf{x})=\frac{1}{2}[\mathbf{P}\mathbf{a}^{(k)}(\mathbf{x})-\mathbf{u}^{(k)}]^T\mathbf{W}[\mathbf{P}\mathbf{a}^{(k)}(\mathbf{x})-\mathbf{u}^{(k)}], \tag{3.6}$$

where

$$\mathbf{P}=\begin{bmatrix}\mathbf{p}^T(\mathbf{x}_1)\\ \mathbf{p}^T(\mathbf{x}_2)\\ \vdots\\ \mathbf{p}^T(\mathbf{x}_{N_t})\end{bmatrix}_{N_t\times m},\qquad \mathbf{W}=\begin{bmatrix}w(\mathbf{x}-\mathbf{x}_1) & \cdots & \mathbf{0}\\ \cdots & \ddots & \cdots\\ \mathbf{0} & \cdots & w(\mathbf{x}-\mathbf{x}_{N_t})\end{bmatrix}_{N_t\times N_t},$$

and

$$\mathbf{u}^{(k)}=[u_1{}^{(k)},u_2{}^{(k)},\cdots,u_{N_t}{}^{(k)}]^T.$$

Here, it should be noted that $u^{(k)}$ is the fictitious nodal values, and not the nodal values of the unknown trial function $u_h^{(k)}(\mathbf{x})$ in general. Setting

$$\frac{\partial\mathcal{J}}{\partial\mathbf{a}^{(k)}}=0$$

leads to the following:

$$(\mathbf{P}\mathbf{a}^{(k)}(\mathbf{x})-\mathbf{u}^{(k)})^T\mathbf{W}\mathbf{P}=0. \tag{3.7}$$

https://doi.org/10.4208/aamm.2015.m1085 Published online by Cambridge University Press

Now, findinig transpose of the the whole equation (3.7) yeilds:

$$(\mathbf{WP})^T(\mathbf{Pa}^{(k)}(\mathbf{x})-\mathbf{u}^{(k)})=0. \tag{3.8}$$

This equation can be rewritten as follows:

$$\mathbf{P}^T\mathbf{WPa}^{(k)}(\mathbf{x})-\mathbf{P}^T\mathbf{Wu}^{(k)}=0. \tag{3.9}$$

Finally

$$\mathbf{P}^T\mathbf{WPa}^{(k)}(\mathbf{x})=\mathbf{P}^T\mathbf{Wu}^{(k)}. \tag{3.10}$$

Define moment matrix $\mathbf{A}(\mathbf{x})$ and $\mathbf{B}(\mathbf{x})$ matrix like follows:

$$\mathbf{A}(\mathbf{x})=\mathbf{P}^T\mathbf{WP}=\sum_{i=1}^{N_t}w(\mathbf{x}-\mathbf{x}_i)\mathbf{p}(\mathbf{x}_i)\mathbf{p}^T(\mathbf{x}_i), \tag{3.11a}$$

$$\mathbf{B}(\mathbf{x})=\mathbf{P}^T\mathbf{W}=[w(\mathbf{x}-\mathbf{x}_1)\mathbf{p}(\mathbf{x}_1),w(\mathbf{x}-\mathbf{x}_2)\mathbf{p}(\mathbf{x}_2),\cdots,w(\mathbf{x}-\mathbf{x}_{N_t})\mathbf{p}(\mathbf{x}_{N_t})]. \tag{3.11b}$$

Using these definitions equation (3.10) becomes

$$\mathbf{A}(\mathbf{x})\mathbf{a}^{(k)}(\mathbf{x})=\mathbf{B}(\mathbf{x})\mathbf{u}^{(k)}. \tag{3.12}$$

Solving for the unknown coeffiecints $\mathbf{a}^{(k)}(\mathbf{x})$

$$\mathbf{a}^{(k)}(\mathbf{x})=\mathbf{A}^{-1}(\mathbf{x})\mathbf{B}(\mathbf{x})\mathbf{u}^{(k)}, \tag{3.13}$$

substituting it into Eq. (3.3), the MLS approximation are usually written as

$$u_h^{(k)}(\mathbf{x})=\sum_{i=1}^{N_t}\phi_i(\mathbf{x})u_i^{(k)}=\mathbf{\Phi}^T(\mathbf{x})\mathbf{u}^{(k)},\quad \mathbf{x}\in\bar{\Omega}, \tag{3.14}$$

where

$$\mathbf{\Phi}^T(\mathbf{x})=\mathbf{p}^T(\mathbf{x})\mathbf{A}^{-1}(\mathbf{x})\mathbf{B}(\mathbf{x}). \tag{3.15}$$

Shape function derivatives can be obtained by application of the product rule on Eq. (3.15)

$$\mathbf{\Phi}_{,k}^T(\mathbf{x})=\mathbf{p}_{,k}^T\mathbf{A}^{-1}\mathbf{B}+\mathbf{p}^T\mathbf{A}_{,k}^{-1}\mathbf{B}+\mathbf{p}^T\mathbf{A}^{-1}\mathbf{B}_{,k}, \tag{3.16}$$

with

$$\mathbf{A}_{,k}^{-1}=-\mathbf{A}^{-1}\mathbf{A}_{,k}\mathbf{A}^{-1}, \tag{3.17}$$

where

$$\mathbf{A}_{,k}(\mathbf{x})=\sum_{i=1}^{N_t}w_{,k}(\mathbf{x}-\mathbf{x}_i)\mathbf{p}(\mathbf{x}_i)\mathbf{p}^T(\mathbf{x}_i). \tag{3.18}$$

https://doi.org/10.4208/aamm.2015.m1085 Published online by Cambridge University Press

The element free Galerkin method only needs to the first derivatives of the MLS shape functions, therefore, here we have discarded the second derivatives of the shape functions. The interested reader can be refer to [43] for the second derivatives of MLS approximation. A similar procedure can be written for approximation $v^{(k)}(\mathbf{x})=v(\mathbf{x},k\Delta t)$ as

$$v_h^{(k)}(\mathbf{x})=\sum_{i=1}^{N_t}\phi_i(\mathbf{x})v_i^{(k)}=\mathbf{\Phi}^T(\mathbf{x})\mathbf{v}^{(k)},\quad \mathbf{x}\in\bar{\Omega}. \tag{3.19}$$

The MLS approximation is well defined only when the moment matrix $\mathbf{A}(\mathbf{x})$ is invertible. It is occurred if and only if the rank of $\mathbf{p}$ matrix equals to m. A necessary condition for a well defined MLS approximation is that at least m weight functions be non-zero for each sample point $\mathbf{x}\in\overline{\Omega}$. Here a sample point may be a quadrature point or nodal point under consideration. Also, the smoothness of the shape functions $\phi_i(\mathbf{x})$ is determined by that of the weight functions [1]. The element free Galerkin method uses the MLS shape functions as the test and trial functions, because of Galerkin method.

3.2.2 The governing system

To express the details of the method, the Schnakenberg model is considered,

$$\frac{\partial u}{\partial t}=\gamma\Big(a-u+u^2v\Big)+\nabla^2u, \tag{3.20a}$$

$$\frac{\partial v}{\partial t}=\gamma\Big(b-u^2v\Big)+d\nabla^2v. \tag{3.20b}$$

The Eqs. (3.2a) and (3.2b) can be simplified to

$$\begin{aligned}&u^{(k+1)}-\beta\Big(\nabla^2u^{(k+1)}+\gamma\Big(-u^{(k+1)}+(u^{(k+1)})^2v^{(k+1)}\Big)\Big)\\&=u^{(k)}+\beta\Big(\nabla^2u^{(k)}+\gamma\Big(-u^{(k)}+(u^{(k)})^2v^{(k)}\Big)\Big)+2\beta\gamma a,\end{aligned} \tag{3.21a}$$

$$\begin{aligned}&v^{(k+1)}-\beta\Big(d\nabla^2v^{(k+1)}-\gamma(u^{(k+1)})^2v^{(k+1)}\Big)\\&=v^{(k)}+\beta\Big(d\nabla^2v^{(k)}-\gamma(u^{(k)})^2v^{(k)}\Big)+2\beta\gamma b,\end{aligned} \tag{3.21b}$$

on which $\beta=\Delta t/2$. To find the EFG shape functions, n nodal points $\{\mathbf{x}_j\}_{j=1}^{N_t}$ in the domain of the problem and on its boundary is considered as MLS nodal points. Substituting (3.14) and (3.19) into Eqs. (3.21a) and (3.21b) and using the shape functions as test functions leads to:

$$\begin{aligned}&\int_\Omega u_j^{(k+1)}\phi_i d\Omega-\beta\int_\Omega\Big(\nabla^2u_j^{(k+1)}+\gamma\Big(-u_j^{(k+1)}+(u_j^{(k+1)})^2v_j^{(k+1)}\Big)\Big)\phi_i d\Omega\\&=\int_\Omega u_j^{(k)}\phi_i d\Omega+\beta\int_\Omega\Big(\nabla^2u_j^{(k)}+\gamma\Big(-u_j^{(k)}+(u_j^{(k)})^2v_j^{(k)}\Big)\Big)\phi_i d\Omega+2\beta\gamma a\int_\Omega\phi_i d\Omega,\end{aligned} \tag{3.22a}$$

https://doi.org/10.4208/aamm.2015.m1085 Published online by Cambridge University Press

$$\int_\Omega v_j^{(k+1)}\phi_i d\Omega-\beta\int_\Omega\left(d\nabla^2 v_j^{(k+1)}-\gamma(u_j^{(k+1)})^2 v_j^{(k+1)}\right)\phi_i d\Omega$$
$$=\int_\Omega v_j^{(k)}\phi_i d\Omega+\beta\int_\Omega\left(d\nabla^2 v_j^{(k)}-\gamma(u_j^{(k)})^2 v_j^{(k)}\right)\phi_i d\Omega+2\beta\gamma b\int_\Omega\phi_i d\Omega, \tag{3.22b}$$

where

$$u_j^{(k)}=u(\mathbf{x}_j,t^{(k)}),\quad v_j^{(k)}=v(\mathbf{x}_j,t^{(k)}),\qquad \mathbf{x}_j\in\text{int}(\Omega),$$
$$\nabla^2 u_j^{(k)}=\sum_{i=1}^{N_t}\left(\frac{\partial^2\phi_i}{\partial x^2}(\mathbf{x}_j)+\frac{\partial^2\phi_i}{\partial y^2}(\mathbf{x}_j)\right)u_i^{(k)},$$
$$\nabla^2 v_j^{(k)}=\sum_{i=1}^{N_t}\left(\frac{\partial^2\phi_i}{\partial x^2}(\mathbf{x}_j)+\frac{\partial^2\phi_i}{\partial y^2}(\mathbf{x}_j)\right)v_i^{(k)}.$$

Therefore Eqs. (3.22a)-(3.22b) constitute a $2N_t\times 2N_t$ system of nonlinear equation on the unknowns $u_i^{(k+1)}$ and $v_i^{(k+1)}$ for $i=1,2,\cdots,N_t$. The values of $u_i^{(k)}$ and $v_i^{(k)}$ are known from the previous time level. At the first time level, i.e., when $k=0$, $u_i^{(0)}$ and $v_i^{(0)}$ are computed by the initial conditions. At each time level a predicator-corrector technique is used to solve the nonlinear equations. The linear equations

$$\int_\Omega u_j^{(k+1)}\phi_i d\Omega-\beta\int_\Omega\left(\nabla^2 u_j^{(k+1)}+\gamma\left(-u_j^{(k+1)}+u_j^{(k+1)}\tilde{u}_j\tilde{v}_j\right)\right)\phi_i d\Omega$$
$$=\int_\Omega u_j^{(k)}\phi_i d\Omega+\beta\int_\Omega\left(\nabla^2 u_j^{(k)}+\gamma\left(-u_j^{(k)}+(u_j^{(k)})^2 v_j^{(k)}\right)\right)\phi_i d\Omega+2\beta\gamma a\int_\Omega\phi_i d\Omega, \tag{3.23a}$$
$$\int_\Omega v_j^{(k+1)}\phi_i d\Omega-\beta\int_\Omega\left(d\nabla^2 v_j^{(k+1)}-\gamma v_j^{(k+1)}(\tilde{u}_j)^2\right)\phi_i d\Omega$$
$$=\int_\Omega v_j^{(k)}\phi_i d\Omega+\beta\int_\Omega\left(d\nabla^2 v_j^{(k)}-\gamma(u_j^{(k)})^2 v_j^{(k)}\right)\phi_i d\Omega+2\beta\gamma b\int_\Omega\phi_i d\Omega, \tag{3.23b}$$

in which $\tilde{u}_j=u_j^{(k)}$ and $\tilde{v}_j=v_j^{(k)}$, yields the linear system,

$$\begin{bmatrix}\mathbf{K}_1+\mathbf{E}-\mathbf{P}_1+\mathbf{G}\\ \mathbf{K}_2+\mathbf{E}+\mathbf{P}_2\end{bmatrix}\begin{bmatrix}\mathbf{u}^{(k+1)}\\ \mathbf{v}^{(k+1)}\end{bmatrix}=\begin{bmatrix}-\mathbf{K}_1+\mathbf{E}+\mathbf{P}_3-\mathbf{G}\\ -\mathbf{K}_2+\mathbf{E}-\mathbf{P}_3\end{bmatrix}\begin{bmatrix}\mathbf{u}^{(k)}\\ \mathbf{v}^{(k)}\end{bmatrix}+\begin{bmatrix}\mathbf{F}_1\\ \mathbf{F}_2\end{bmatrix}, \tag{3.24}$$

where

$$K_{ij}=\int_\Omega\nabla\phi_i\cdot\nabla\phi_j d\Omega,\qquad \mathbf{K}_1=\beta\mathbf{K},\qquad \mathbf{K}_2=d\beta\mathbf{K}, \tag{3.25a}$$
$$E_{ij}=\int_\Omega\phi_i\cdot\phi_j d\Omega,\qquad \mathbf{G}=\beta\gamma\mathbf{E}, \tag{3.25b}$$
$$P_{1_{ij}}=\beta\gamma\tilde{u}_j\tilde{v}_j\mathbf{E},\qquad P_{2_{ij}}=\beta\gamma\tilde{u}_j^2\mathbf{E},\qquad P_{3_{ij}}=\beta\gamma\tilde{u}_j^{(k)}\tilde{v}_j^{(k)}\mathbf{E}, \tag{3.25c}$$

https://doi.org/10.4208/aamm.2015.m1085 Published online by Cambridge University Press

and

$$\mathbf{F}_i = \int_\Omega \phi_i d\Omega, \qquad \mathbf{F}_1 = 2\beta\gamma a\mathbf{F}, \qquad \mathbf{F}_2 = 2\beta\gamma b\mathbf{F}. \tag{3.26}$$

To find this system the Divergence theorem is applied. The absence of boundary integrals is because of the homogenous Neumann boundary conditions:

$$\sum_{i=1}^{N_t} \frac{\partial \phi_i}{\partial n_p}(\mathbf{x}_j) u_i^{(k+1)} = 0, \quad \mathbf{x}_j \in \partial\Omega, \tag{3.27}$$

and

$$\sum_{i=1}^{N_t} \frac{\partial \phi_i}{\partial n_p}(\mathbf{x}_j) v_i^{(k+1)} = 0, \quad \mathbf{x}_j \in \partial\Omega. \tag{3.28}$$

The EFG method requires the partitioning of the domain into cell integration. To evaluate all integrals appeared in Eqs. (3.25a)-(3.26), Gaussian quadrature rules are used in a background mesh or cell structure. In [17] integration on triangular and quadrilateral elements is explained. A perfect description of EFGM implementation is given by Belytschko in [6]. The integration accuracy can be improved by aligning the integration cell with the support of the integrand [9].

At first the linear system (3.24) is solved for unknowns $u_i^{(k+1)}$ and $v_i^{(k+1)}$ for $i = 1,2,\cdots,N_t$, assuming that the values of the $u_i^{(k)}$ and $v_i^{(k)}$ are known from the previous time level. Then $\tilde{u}_j = u_j^{(k+1)}$ and $\tilde{v}_j = v_j^{(k+1)}$ is put in the system (3.24) where $u_j^{(k+1)}$ and $v_j^{(k+1)}$ are just obtained and recompute $u_i^{(k+1)}$ and $v_i^{(k+1)}$ for $i = 1,2,\cdots,N_t$. This procedure is iterated until all unknown quantities converge to within a prescribed number of significant figures. When the prescribed convergence is achieved, we can move on to the following time level. The resulting solution from the current time level, provides the known values for the next time step. This process is repeated, until it approaches to the desirable time t. When $u(\mathbf{x}_j,t)$ and $v(\mathbf{x}_j,t)$, for all nodes $\{\mathbf{x}_j\}_{j=1}^{N_t}$, are obtained, the values of $u(\mathbf{x},t)$ and $v(\mathbf{x},t)$, at any point $\mathbf{x}$ in the problem domain Ω, are approximated using Eqs. (3.14) and (3.19), respectively as

$$u_h(\mathbf{x},t) = \sum_{i=1}^{N_t} \phi_i(\mathbf{x}) u(\mathbf{x}_i,t), \quad v_h(\mathbf{x},t) = \sum_{i=1}^{N_t} \phi_i(\mathbf{x}) v(\mathbf{x}_i,t), \quad \mathbf{x} \in \bar{\Omega}. \tag{3.29}$$

A similar approach could be used to discretize other reaction-diffusion systems.

4 The numerical investigations

In this section, the element free Galerkin method is applied for two reaction-diffusion systems. In all cases the quadratic basis $(m = 6)$ and the cubic spline weight function

https://doi.org/10.4208/aamm.2015.m1085 Published online by Cambridge University Press

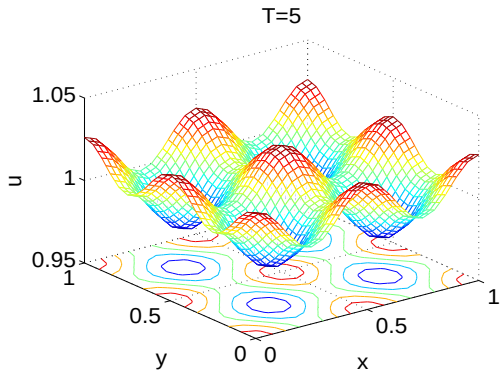


Figure 1: Numerical solution of the Schnakenberg model on the unit square with parameters $a=0.1$, $b=0.9$, $d=8.6676$ and $\gamma=435.99$. The solution surface of the activator u at $T=5$.

with rectangular support are used:

$$w(r)=\begin{cases} 2/3-4r^2+4r^3, & r\leq 1/2, \\ 4/3-4r+4r^2-4/3r^3, & 1/2<r\leq 1, \\ 0, & r>1, \end{cases} \tag{4.1}$$

where $r=\frac{|\mathbf{x}-\mathbf{x}_i|}{d_i}$, in which d_i is the support size of node i. The number of nodes is stated in each case. In all examples when the problem domain is square or rectangular, the cell structure (square mesh) with 4×4 Gaussian points in each cell is considered. Other problem domains partitioned by triangle mesh and 6 Gaussian points rule is used to evaluate integrals on each triangle. It is important to say that to evaluate the integrals numerically, one has to find MLS shape functions and their first derivatives at each Gaussian points. Therefore, it cause this method has a little high computational cost. So, due to high computational cost of the element free Galerkin method, it seems using the 4×4 on square cell and 6 on triangles are good choices. Also, the nodes on the boundaries are distributed such that the distance between them are almost equal to distance between other nodes. In this paper, the contour profiles of the solutions is plotted only. This is mainly for biological interpretation. In the biological context color patterns are linked to cell differentiation. Assuming that coloration is determined by a constant threshold value in u (or v) concentration, u_s (or v_s) say, such that cells in the region where $u\geq u_s$ are blue, while cells which experience a concentration $u<u_s$ are colored white, these give rise to the shading illustrated in all the figures. The actual solution surface u with parameters $a=0.1$, $b=0.9$, $d=8.6676$ and $\gamma=435.99$ is as depicted in Fig. 1.

4.1 Schnakenberg model

4.1.1 Example 1

As the first numerical experiment, we consider the Schnakenberg model equations (2.4a) and (2.4b) on the unit square domain $\Omega=(0,1)^2$ with homogenous Neumann boundary

https://doi.org/10.4208/aamm.2015.m1085 Published online by Cambridge University Press

Table 2: CPU time and error of EFG method applied to the Schnakenberg model in the unit square domain $(0,1)^2$, at $T=3$.

Δt	CPU time (s)	L^∞ error
5e-3	284	2.07E-05
2.5e-3	432	3.01E-05
1e-3	704	2.42E-05

conditions applied to both u and v. From the linear stability analysis this system has a uniform positive steady state (u_s,v_s) given by $u_s=a+b$ and $v_s=b/(a+b)^2$, with $a\geq 0$ and $a+b\geq 0$. Let the parameter values $a=0.1$, $b=0.9$, $d=8.6676$ and $\gamma=114$. So $(u_s,v_s)=(1,0.9)$ is the homogeneous steady state of this problem. Initial conditions are taken as small random perturbations around this steady state.

In computations 441 uniformly distributed nodes in the problem domain $\Omega=(0,1)^2$ and on its boundary are used. The criterion for convergence to the inhomogeneous steady state is regarded as

$$E_u^{(k)}=\frac{\|\mathbf{u}^{(k+1)}-\mathbf{u}^{(k)}\|_\infty}{\|\mathbf{u}^{(k+1)}\|_\infty}<\epsilon,$$

in which $\epsilon=10^{-6}$. To show better the efficiency of the present method, in all examples with initial conditions randomly perturbed around this steady state, the initial conditions for $\mathbf{u}_{\Delta t}$ are saved and used as initial conditions for $\mathbf{u}_{2\Delta t}$, too. In this case the inhomogeneous steady state is close to $T=3$. To study the performance and convergence of the element free Galerkin method, the CPU time and error for simulations of the Schnakenberg model is reported in Table 2. The error at Δt is measured as a difference between this solution, $\mathbf{u}_{\Delta t}$, and the solution $\mathbf{u}_{2\Delta t}$ for time step size $2\Delta t$ at $T=3$, i.e.,

$$E_{\Delta t}=\|\mathbf{u}_{\Delta t}-\mathbf{u}_{2\Delta t}\|_\infty. \tag{4.2}$$

The time evolution of the activator concentration u is shown in Fig. 2. We can observe that the initial random perturbation is amplified and spreads, leading to formation of striped pattern presented in Fig. 2. Moreover to study the effect of varying γ, all parameter values a, b, d is fixed and resolve the equation with $\gamma=230.82$, $\gamma=329.20$, $\gamma=666.82$ and $\gamma=435.99$. Fig. 4 shows the numerical simulations obtained by these values of γ.

4.1.2 Example 2

Consider the Schnakenberg model equations (2.4a) and (2.4b) with homogenous Neumann boundary conditions applied to both u and v as before. Following the setup in [18], the initial conditions are taken as

$$u(x,y,0)=a+b+10^{-3}\exp\Big(-100\Big(\Big(x-\frac{1}{3}\Big)^2+\Big(y-\frac{1}{2}\Big)^2\Big)\Big), \tag{4.3a}$$

$$v(x,y,0)=\frac{b}{(a+b)^2}, \tag{4.3b}$$

https://doi.org/10.4208/aamm.2015.m1085 Published online by Cambridge University Press

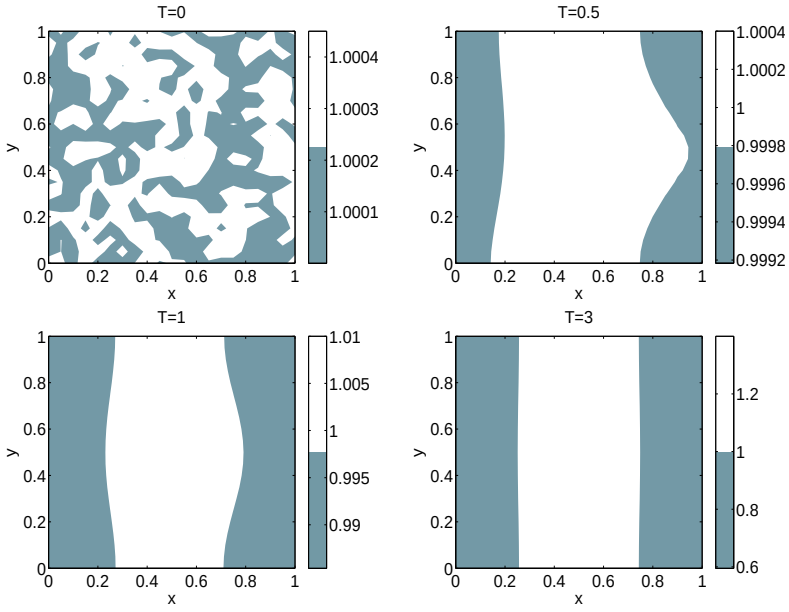


Figure 2: Numerical solution of the Schnakenberg model on the unit square with parameters $a=0.1$, $b=0.9$, $d=10$ and $\gamma=114$. Contour plots of time evolution of the activator u at different times.

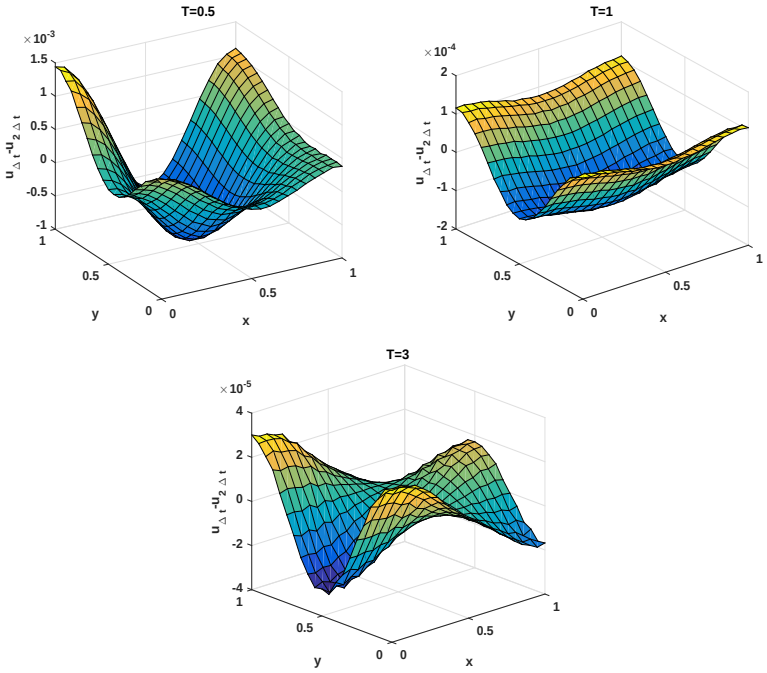


Figure 3: Error $u_{\Delta t}-u_{2\Delta t}$ of the Schnakenberg model on the unit square with parameters $a=0.1$, $b=0.9$, $d=10$ and $\gamma=114$ for $T=0.5$, $T=1$ and $T=3$.

https://doi.org/10.4208/aamm.2015.m1085 Published online by Cambridge University Press

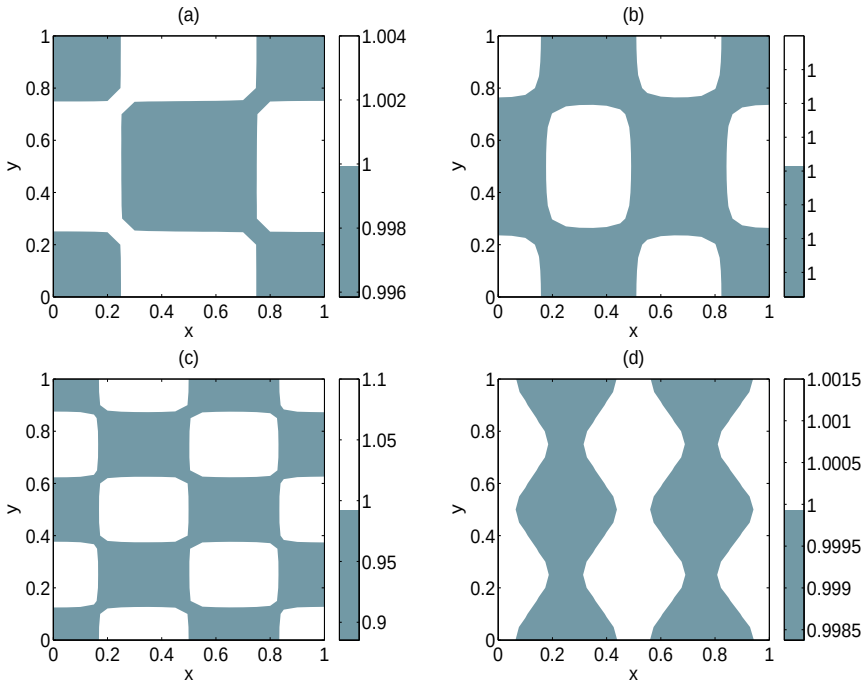


Figure 4: Contour plots of the activator u of the Schnakenberg model on the unit square with parameters $a=0.1$, $b=0.9$, $d=8.6676$ and (a) $\gamma=230.82$, (b) $\gamma=329.20$, (c) $\gamma=666.82$ and $\gamma=435.99$.

and the parameter values are $a=0.1305$, $b=0.7695$, $d=8.6676$ and $\gamma=666.82$. Firstly, the equations on the unit square domain $\Omega=(0,1)^2$ are considered. The time evolution of the activator u obtained by 441 nodes is shown in Fig. 5. It can be observe that the initial perturbation in (4.3a) and (4.3b) is amplified and spreads, leading to formation of spot-like patterns. Next, we vary the shape and size of the domain, but all parameters are kept unchanged. The time evolution plots of activator concentrations u are shown in Fig. 6 for the circular domain $\Omega=\{(x,y)|(x-0.5)^2+(y-0.5)^2<0.5^2\}$ and in Fig. 7 for the elliptical domain $\Omega=\{(x,y)|(\frac{x-0.5}{0.25})^2+(\frac{y-0.5}{0.5})^2<1\}$. In Schnakenberg model 288 nodes in the circular domain and 222 nodes in the elliptical domain are used.

Also, the CPU time and error for simulations of the Schnakenberg model on the circular domain is reported at $T=5$ in Table 3, where is close to steady state.

Table 3: CPU time and error of EFG method applied to the Schnakenberg model in the circular domain, at $T=5$.

Δt	CPU time (s)	L^∞ error
1e-3	399	8.51E-04
5e-4	601	6.86E-04
2.5e-4	1067	9.47E-04

https://doi.org/10.4208/aamm.2015.m1085 Published online by Cambridge University Press

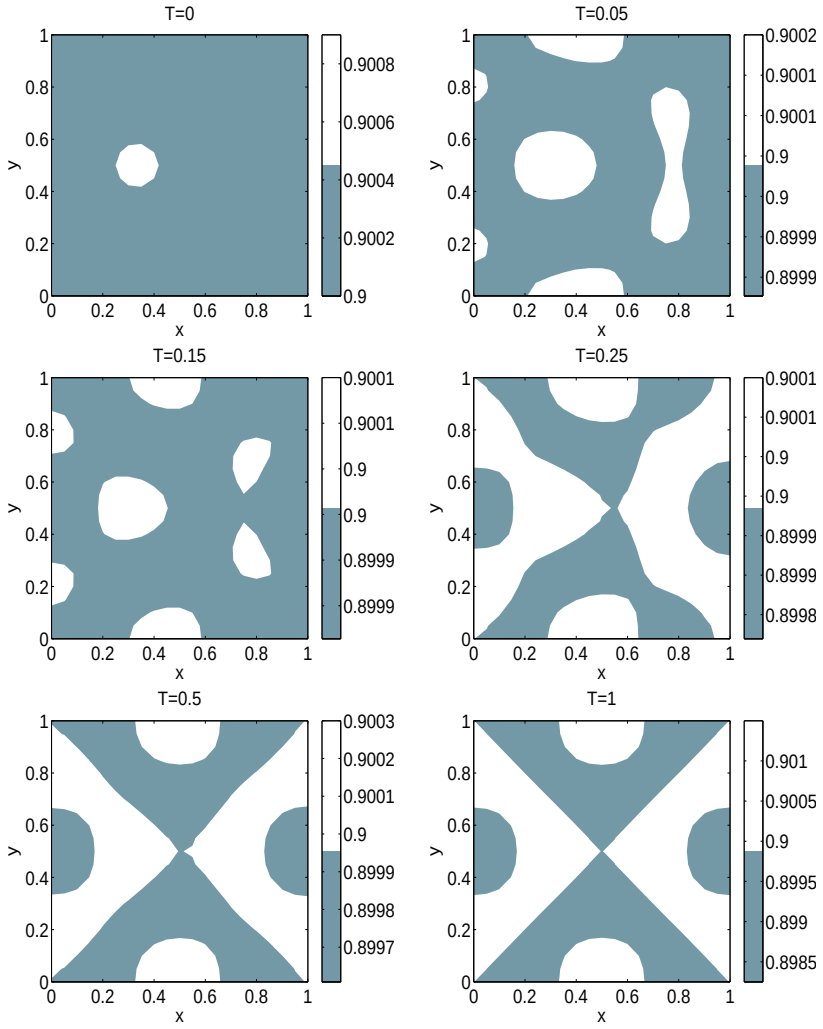


Figure 5: Numerical solution of the Schnakenberg model on the unit square with parameters $a=0.1305$, $b=0.7695$, $d=8.6676$ and $\gamma=666.82$. Contour plots of time evolution of the activator u at different times.

4.2 Gierer-Meinhardt model

4.2.1 Example 3

In this example the Gierer-Meinhardt reaction kinetics is solved with homogenous Neumann boundary conditions for both u and v. Initial conditions are taken as random perturbations about a constant value. The parameter values a=0.1, b=1.0, K=0.5, d=75.1573, $\gamma=483.43$ are fixed and only vary the shape of the domain.

The time evolution plots of activator u are shown in Fig. 8 for a square domain with 441 nodes, Fig. 9 for a circular domain with 185 nodes and Fig. 10 for an elliptical domain with 157 nodes. Also the time evolution plots of activator u are shown in Fig. 11 for a

https://doi.org/10.4208/aamm.2015.m1085 Published online by Cambridge University Press

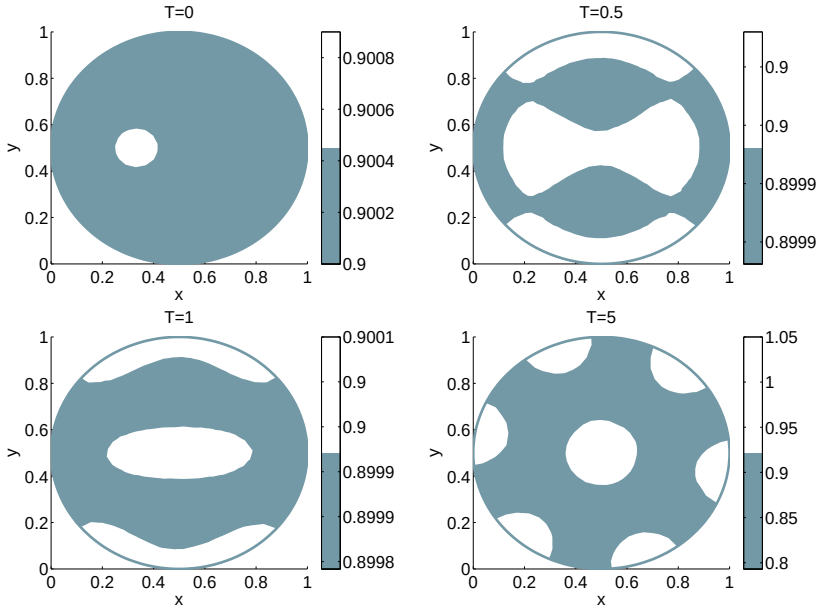


Figure 6: Numerical solution of the Schnakenberg model on a circular domain with parameters $a=0.1305$, $b=0.7695$, $d=8.6676$ and $\gamma=666.82$. Contour plots of time evolution of the activator u at different times.

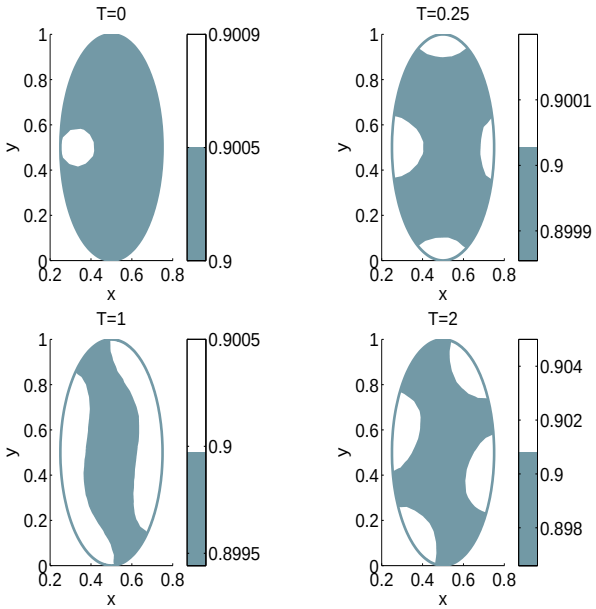


Figure 7: Numerical solution of the Schnakenberg model on an elliptical domain with parameters $a=0.1305$, $b=0.7695$, $d=8.6676$ and $\gamma=666.82$. Contour plots of time evolution of the activator u at different times.

https://doi.org/10.4208/aamm.2015.m1085 Published online by Cambridge University Press

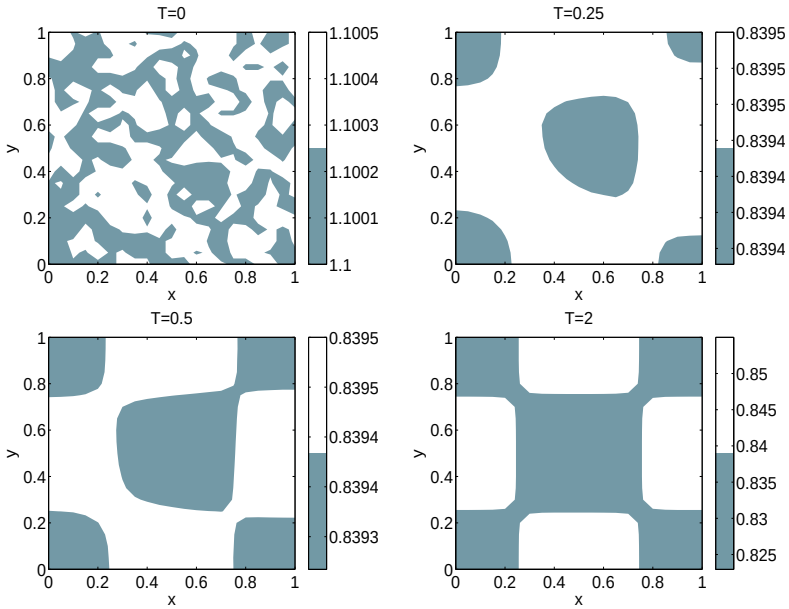


Figure 8: Numerical solution of the Gierer-Meinhardt model on a square domain with parameters $a=0.1$, $b=1.0$, $K=0.5$, $d=75.1573$ and $\gamma=483.43$. Contour plots of time evolution of the activator u at different times.

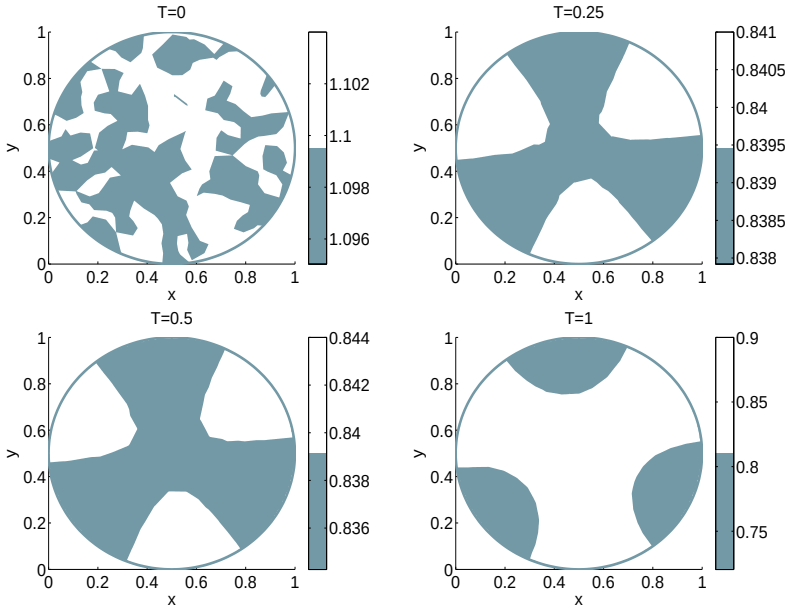


Figure 9: Numerical solution of the Gierer-Meinhardt model on a circular domain with parameters $a=0.1$, $b=1.0$, $K=0.5$, $d=75.1573$ and $\gamma=483.43$. Contour plots of time evolution of the activator u at different times.

https://doi.org/10.4208/aamm.2015.m1085 Published online by Cambridge University Press

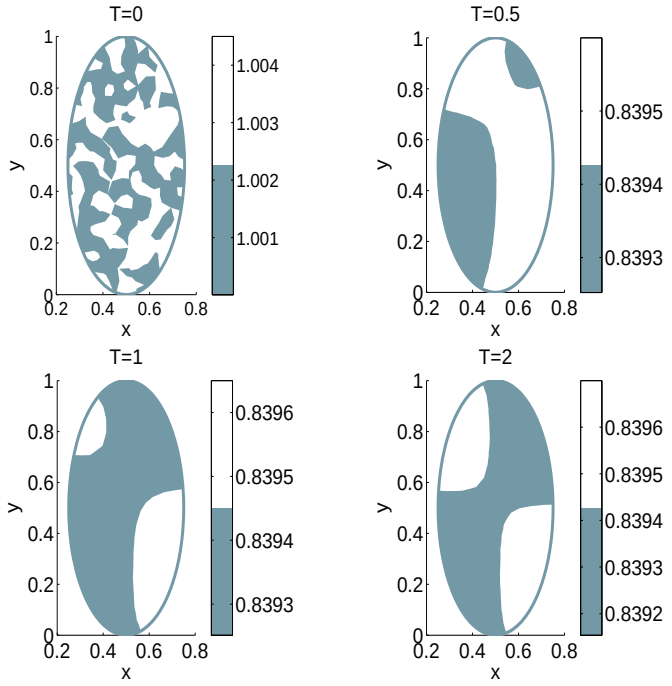


Figure 10: Numerical solution of the Gierer-Meinhardt model on a elliptical domain with parameters $a=0.1$, $b=1.0$, $K=0.5$, $d=75.1573$ and $\gamma=483.43$. Contour plots of time evolution of the activator u at different times.

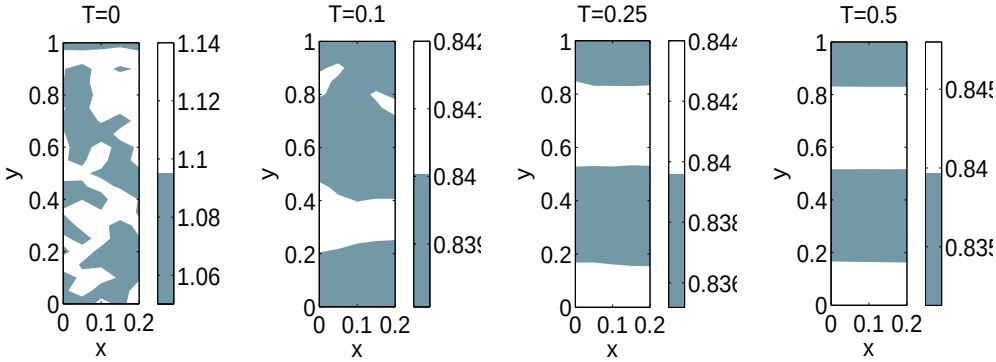


Figure 11: Numerical solution of the Gierer-Meinhardt model on a rectangular domain with parameters $a=0.1$, $b=1.0$, $K=0.5$, $d=75.1573$ and $\gamma=483.43$. Contour plots of time evolution of the activator u at different times.

narrow rectangular domain with 110 nodes that leads to a stripe pattern.

These simulations of the Gierer-Meinhardt system on different domains provide an example of the sensitivity of patterns in reaction-diffusion systems with respect to the domain size and shape. The CPU time and error for simulations of the Gierer-Meinhardt model is shown in Table 4 on the unit square at $T=2$ and Table 5 on the circular domain at $T=1$.

https://doi.org/10.4208/aamm.2015.m1085 Published online by Cambridge University Press

Table 4: CPU time and error of EFG method applied to the Gierer-Meinhardt model in the unit square, at $T=2$.

Δt	CPU time (s)	L^∞ error
1e-3	570	1.40E-04
5e-4	822	1.72E-04
2.5e-4	1039	8.10E-04

Table 5: CPU time and error of EFG method applied to the Gierer-Meinhardt model in the circular domain, at $T=1$.

Δt	CPU time (s)	L^∞ error
1e-3	49	1.55E-02
5e-4	58	1.58 E-02
2.5e-4	87	2.39 E-03

5 Conclusions

In this paper the numerical solution of the reaction-diffusion systems in fix domains has been studied using the element free Galerkin method. The numerical solutions for two species, the Schnakenberg and the Gierer-Meinhardt models have been presented in different regions to demonstrate the effects of various geometrical domains on the resulting biological patterns. The EFG method is not a truly meshfree method, it requires a background cell for integrations, but does not need to mesh for approximation. Our numerical examples show good results. Although this method needs high number of Gaussian points to get a good accuracy, but comparison between the results of the current method and the FPM [39] shows that the number of utilized nodes in the EFG method is very fewer than the FPM. Obviously, the reason is the use of the weak form of equations in the EFG method. Also most of the time the inhomogeneous steady state is found by fewer time steps. Moreover, by a comparison between existent works [39] and [37], it seems that number of iterations in finite volume spectral element method is much more than both FPM and EFGM to get reasonable results. But the author have used few number of nodes in finite volume spectral element method than these two works by FPM ad EFGM.

Acknowledgments

We thank both the anonymous referees for carefully reading the paper and their comments and suggestions. The second author was in part supported by a grant from IPM (No. 95650422).

References

[1] S. N. ATLURI AND T. ZHU, *A modified collocation method and a penalty formulation for enforcing*

https://doi.org/10.4208/aamm.2015.m1085 Published online by Cambridge University Press

the essential boundary conditions in the element free Galerkin method, Comput. Mech., 21 (1998), pp. 211–222.

[2] S. N. ATLURI AND T. ZHU, *A new meshless local petrov-Galerkin (MLPG) approach in computational mechanics,* Comput. Mech. 22 (1998), pp. 117–127.

[3] S. N. ATLURI AND S. SHEN, The Meshless Local Petrov-Galerkin (MLPG) Method, Tech Science Press, 2002.

[4] S. R. BARRIO, C. VAREA, J. ARAGON AND P. MAINI, *A two-dimensional numerical study of spatial pattern formation in interacting systems,* Bull. Math. Biol., 61 (1999), pp. 483–505.

[5] M. BAURMANNA, T. GROSS AND U. FEUDEL, *Instabilities in spatially extended predator-prey systems: spatio-temporal patterns in the neighborhood of Turing-Hopf bifurcations,* J. Theor. Biol., 245 (2007), pp. 220–229.

[6] T. BELYTSCHKO, Y. LU AND L. GU, *Element free Galerkin methods,* Int. J. Num. Meth. Eng., 37 (1994), pp. 229–256.

[7] M. CHAPLAIN, A. GANESH AND I. GRAHAM, *Spatio-temporal pattern formation on spherical surfaces: numerical simulation and application to solid tumor growth,* J. Math. Biol., 42 (2001), pp. 387–423.

[8] E. CRAMPIN, E. GAFFNEY AND P. MAINI, *Reaction and diffusion on growing domains: Scenarios for robust pattern formation,* Bull. Math. Biol., 61 (1999), pp. 1093–1120.

[9] J. DOLBOW AND T. BELYTSCHKO, *Numerical integration of the Galerkin weak form in meshfree methods,* Comput. Mech., 23 (1999), pp. 219–230.

[10] J. DOLBOW AND T. BELYTSCHKO, *An introduction to programming the meshless element free Galerkin method,* Comput. Meth. Eng., 5(3) (1998), pp. 207–241.

[11] C. A. DUARTE AND J. T. ODEN, *An hp adaptive method using clouds,* Comput. Methods Appl. Mech. Eng., 139 (1996), pp. 237–262.

[12] S. FERREIRA, M. MARTINS AND M. VILELA, *Reaction-diffusion model for the growth of avascular tumor,* Phys. Rev., 65(2) (2002), pp. 1467–1476.

[13] H. FREDERIK, P. MAINI, A. MADZVAMUSE, A. WATHEN AND T. SEKIMURA, *Pigmentation pattern formation in butterflies: experiments and models,* C. R. Biol., 326 (2003), pp. 717–727.

[14] J. GARCÍA-AZNAR, J. KUIPER, M. GÓMEZ-BENITO, M. DOBLARÉ AND J. RICHARDSON, *Computational simulation of fracture healing: influence of interfragmentary movement on the callus growth,* J. Biomech., 40 (2007), pp. 1467–1476.

[15] D. A. GARZÓN-ALVARADO, C. H. GALEANO AND J. M. MANTILLA, *Turing pattern formation for reaction-convection-diffusion systems in fixed domains submitted to toroidal velocity fields,* Appl. Math. Model., 35 (2011), pp. 4913–4925.

[16] A. GIERER AND H. MEINHARDT, *A theory of biological pattern formation,* Kybernetik, 12 (1972), pp. 30–39.

[17] M. S. GOCKENBACH, Understanding and Implementing the Finite Element Method, SIAM, 2006.

[18] W. HUNDSDORFER AND J. VERWER, Numerical Solution of Time-Dependent Advection-Diffusion-Reaction Equations, Springer, Berlin, 2003.

[19] A. KASSAM AND L. TREFETHEN, *Solving reaction-diffusion equations 10 times faster,* Oxford University: Numerical Analysis Group Research, Report 16, 2003.

[20] S. KONDO AND R. ASAI, *A reaction-diffusion wave on the skin of the marine anglefish Pomacanthus,* Nature, 376 (1995), pp. 765–768.

[21] P. LANCASTER AND K. SALKAUSKAS, *Surface generated by moving least squares methods,* Math. Comput., 37 (1981), pp. 141–158.

[22] W. K. LIU, S. JUN, S. LI, J. ADEE AND T. BELYTSCHKO, *Reproducing kernel particle methods*

https://doi.org/10.4208/aamm.2015.m1085 Published online by Cambridge University Press

for structural dynamics, Int. J. Num. Meth. Eng., 5(3) (1995), pp. 1655–1679.
[23] W. K. LIU, Y. CHEN, S. JUN, J. S. CHEN, T. BELYTSCHKO, C. PAN, R. A. URAS AND C. T. CHANG, *Overview and applications of the reproducing kernel particle method,* Arch. Comput. Meth. Eng., 3(1) (1996), pp. 3–80.
[24] A. MADZVAMUSE, A Numerical Approach to the Study of Spatial Pattern Formation, Ph.D. Thesis, University of Oxford, 2000.
[25] A. MADZVAMUSE, A. WATHEN AND P. MAINI, *A moving grid finite element method for the simulation of pattern generation by Turing models on growing domains,* J. Sci. Comput., 24 (2005), pp. 247–262.
[26] A. MADZVAMUSE, A. WATHEN AND P. MAINI, *A moving grid finite element method applied to a model biological pattern generator,* J. Comput. Phys., 190 (2003), pp. 478–500.
[27] A. MADZVAMUSE AND P. MAINI, *Velocity-induced numerical solution of reaction-diffusion systems on continuously growing domains,* J. Comput. Phys., 225 (2007), pp. 100–119.
[28] H. MEINHARDT, Models of Biological Pattern Formation, Academic Press, New York, 1982.
[29] J. M. MELENK AND I. BABUSKA, *The partition of unity finite element method: Basic theory and applications,* Comput. Methods Appl. Mech. Eng., 139 (1996), pp. 289–314.
[30] J. J. MONAGHAN, *Smoothed particle hydrodynamics: Some recent improvement and applications,* Annu. Rev. Astron. Phys., 30 (1992), pp. 543–574.
[31] J. D. MURRAY, *A prepattern formation mechanism for animal coat markings,* J. Theor. Biol., 88 (1981), pp. 161–199.
[32] J. D. MURRAY, Mathematical Biology, Springer, Heidelberg, New York, 1993.
[33] B. NAYROLES, G. TOUZOT AND P. VILLON, *Generalizing the FEM: Diffuse approximation and diffuse elements,* Comput. Mech., 10 (1992), pp. 307–318.
[34] E. OÑATE, S. IDELSOHN, O. C. ZIENKIEWICZ AND T. FISHER, *Finite point method for analysis of fluid flow problems,* Proceedings of the 9th Int. Conference on Finite Element Methods in Fluids. Venize, Italy, October, 1995, 15-21.
[35] E. OÑATE, S. IDELSOHN, O. C. ZIENKIEWICZ AND R. L. TAYLOR, *A finite point method in computational mechanics, Applications to convective transport and fluid flow,* Int. J. Num. Meth. Eng., 39 (1996), pp. 3839–3866.
[36] P. W. RANDLES AND L. D. LIBERSKY, *Smoothed particle hydrodynamics: Some recent improvement and applications,* Comput. Methods Appl. Mech. Eng., 139 (1996), pp. 375–408.
[37] F. SHAKERI AND M. DEHGHAN, *The finite volume spectral element method to solve Turing models in the biological pattern formation,* J. Comput. Math. Appl., 32 (2011), pp. 4322–4336.
[38] J. SCHNAKENBERG, *Simple chemical reaction systems with limit cycle behavior,* J. Theoret. Biol., 81 (1979), pp. 389–400.
[39] M. TATARI, M. KAMRANIAN AND M. DEHGHAN, *The finite point method for reaction-diffusion systems in developmental biology,* CMES., 82(1) (2011), pp. 1–27.
[40] D. THOMAS, *Artificial enzyme membrane, transport, memory and oscillatory phenomena,* in: D. Thomas, J.-P. Kervenez (Eds.), Analysis and Control of Immobilised Enzyme Systems, Springer, Berlin, Heidelberg, New York, (1975), pp. 115–150.
[41] A. TURING, *The chemical basis of morphogenesis,* Philos. Trans. Roy. Soc. London, 237 (1952), pp. 37–72.
[42] F. YI, J. WEI AND J. SHI, *Bifurcation and spatiotemporal patterns in a homogeneous diffusive predator-prey system,* J. Differ. Equation, 246(5) (2009), pp. 1944–1977.
[43] L. L. YAW, Co-Rotational Meshfree Formulation for Large Deformation Inelastic Analysis of Two Dimensional Structural Systems, Ph.D. Thesis, University of California, 2008.
[44] T. ZHU, J. D ZHANG AND S. N. ATLURI, *A local boundary integral equation (lbie) method in*

https://doi.org/10.4208/aamm.2015.m1085 Published online by Cambridge University Press

computational mechanics, and a meshless discretization approach, Comput. Mech., 21 (1998), pp. 223–235.

[45] T. ZHU, J. D. ZHANG AND S. N. ATLURI, *A meshless local boundary integral equation (lbie) method for solving nonlinear problems,* Comput. Mech., 22 (1998), pp. 174–186.

https://doi.org/10.4208/aamm.2015.m1085 Published online by Cambridge University Press